Journal of Mining and Environment (JME), Vol. 14, No. 1, 2023, 79-96

Shahrood University of Technology

Journal of Mining and Environment (JME)

Journal homepage: www.jme.shahroodut.ac.ir

Iranian Society of Mining Engineering (IRSME)

Change Detection of Surface Water of Atfih Spring by Integrated Effect of Rainfall Storms and Geological Structures using Landsat Data

Deemah Saad[1]*, Ahmed A. Madani[1], Said M. Said[1], Mohamed Mokhtar Yehia[2] and Tamer Nassar[1]

1. Cairo University, Faculty of Science, Geology Department, Giza, Egypt
2. Central Laboratory for Environmental Quality Monitoring, National Water Research Center, Kanater El-Khairia, Egypt

Article Info

Received 16 December 2022
Received in Revised form 15 January 2023
Accepted 20 January 2023
Published online 20 January 2023

DOI: 10.22044/jme.2023.12516.2272

Keywords

Multi-temporal Landsat Data
Atfih Water Body
Rainfall Storms
Geological Structures

Abstract

The eastern border of the Nile valley south of Cairo is distinguished by numerous springs and associated surface water bodies, e.g. Ain El-Sira, Helwan, and Atfih. Except the latter, all of them were disseminated in urban areas, and were hardly detected by remote sensing data. Thus, studying the surface water of Atfih spring is key to understanding the nature of the east Nile spring system. Change in this surface water has been detected based on the integration between the spatiotemporal analysis of the multi-spectral satellite images and the Modern-Era Retrospective Analysis for Research and Applications (MERRA-2) rainfall data from 1987 to 2019, and the field investigation. The normalized differential water index analysis reveals an increase in the surface area of the Atfih water body by two to three times during the years 2016-2017. The results clarified the relationship between the appearance of the surface water of Atfih spring and rainfall amounts. Another factor controlling the Atfih water body treated in this work is the geological structures. A field survey aided by the processed satellite data revealed the presence of three fault populations: WNW-ESE, E-W to ENE-WSW, and NNE-SSW. The E-W to ENE-oriented faults are the main faults and have a right-lateral strike-slip sense of movement. This fault pattern and Pliocene shale have a substantial impact on the appearance of the Atfih water body. These faults act as a horizontal channel that allows lateral movement of meteoric water through Eocene carbonate, and water recharge occurs at the highly fractured strike-slip transfer zones.

1. Introduction

Egypt lies in a hyper-arid region, and faces severe water scarcity [1], where the Nile is the main source of Egyptian water. The construction of a new dam on the Upper Nile and the continual increase in population and agricultural activities led to the consideration of springs as an alternative supply of water.

Generally, many springs of different types (thermal springs, sulfur springs, mineral springs, and potable spring water) are distributed throughout the Egyptian Desert. These springs exist in Sinai, Western and Eastern Deserts. In Greater Cairo several springs are flowing, such as Ain Mousa, Ain El-Sira, Sulfuric Helwan springs, Ain Helwan, and Ain Atfih [2].

Several authors studied the hydrogeological and hydrogeochemical characteristics of the springs distributed along the east Greater Cairo district. [1], [3]–[5] discussed the hydrogeology of the studied area. [6] discussed hydrogeochemistry of surface water and groundwater from fractured carbonate aquifer. [5] discussed the thermal fluid of Helwan springs by using isotope analysis. [7] studied hydrogeology, hydrogeochemistry, and isotope of the Quaternary aquifer in Atfih area.

Although [7]–[9] studied Atfih area and its surrounding, most of these studies neglect the springs that exist in Atfih area and their water genesis. Atfih surface water spring lies southeast of Atfih city and northeast of the Nile valley. This spring water may be used for Atfih inhabitants' utilizations for industrial or agricultural use such as irrigational use by mixing this water with Nile

Corresponding author: deemah@sci.cu.edu.eg (D. Saad)

water for land reclamation and sustainable development of the area around Atfih city.

Springs are the surface discharge of water from deep-seated groundwater aquifers. Fault damage zones are characterized by intense fracture patterns that allow movements of fluids along strike and dip [10], [11]. The occurrence of springs is governed primarily by the recharge characteristics of the rocks, such as permeability and porosity of the soil, lithology, structure features, and hydrogeomorphology of the surface, as well as precipitation [12]. Generally, water flow patterns in groundwater aquifers are strongly affected by faults (many authors mentioned that, e.g. [10], [13]–[16]). The fault intersection zones, relay ramps, accommodation zones in normal fault zones, step-over zones along strike-slip fault systems, and fault termination zones are the common occurrence of the springs. Additionally, the fault and fracture zones caused the mineralization of the formation, acting as a conductor or tunnel for these deposits [17].

From the last century till now, remote sensing has been the most useful technique for monitoring the change of features and applications that are applied in various fields. Moreover, Landsat satellite imagery series are utilized for change detection studies due to accessibility and cost-effectiveness. Detecting changes in land cover and land use, monitoring climatic change, and the area of surface water bodies, are considered examples of remote sensing applications. Since 1989 there has been a rapid increase in using change detection techniques for many applications. For example [18]–[23]applied a change detection method for monitoring the change of land cover/land use with the time change. [24]–[26] utilized the integration between Geographic Information System (GIS), remote sensing, and change detection techniques to study the change in forest and vegetation. In addition [27]–[32] used multi-satellite images, change detection techniques, and GIS to detect the temporal change of surface waterbodies area. Several applications are used to delineate the surface water bodies with the integration of remote sensing data using single or multi-band techniques. The normalized difference water index (NDWI) is one of the multiband techniques that is applied on the Landsat satellite series to extract the surface water bodies. Many researchers used this index (NDWI) to delineate several surface water bodies for various regions such as[27], [31]–[34]. Thus, why this water body appears? And what are the main factors controlling its appearance? The present paper aims to calculate the surface area of this water body and to clarify the main factors controlling its appearance. This will help improving the water resources in urban areas to reach sustainable cities.

2. Studied Area

The studied area lies 9.5 Km southeast of Atfih city, 74 Km south of Cairo, and covers an area of approximately 110 km^2 (Figure1). It is characterized by a warm winter and hot, dry summers. The annual average of precipitation is 15mm, humidity at 45%, and daily temperature is 29.7ºC, respectively. The main geomorphologic features that cover the studied area are: 1) alluvial plain has an average elevation of about 40m (above the sea level), 2) limestone plateau up to 200m elevation to the east of the study area, 3) isolated hills, and 4) sinkholes karst features. The low land alluvial plain includes deposits of the drainages such as wadi Atfihy and deposits of the Nile floodplain. The drainage network of Wadi El Atfihy and wadi Atfih-1 cut across the structural plateau, terminating westward in the alluvial plain. These drainage networks receive water from occasional heavy rainfall during the winter [35].

3. Geological and Hydrogeological Setting

Several authors studied the geology of Atfih area, among them [35]–[38], [40]–[42]. The exposed lithostratigraphic rock units of the studied area are Middle Eocene Mokattam group, Pliocene Kom El-shelul formation, and Quaternary Wadi deposits (Figure 2). The middle Eocene deposits are exposed in the eastern side of the studied area. The middle Eocene Mokattam group is represented in the studied area by Beni Suef formation at the base and Observatory Formation at the top which is dominated by limestone, marl, and shale sediments. Pliocene rock units are classified into two formations Kom el-Shelul bed and undifferentiated Pliocene bed. Kom el-Shelul formation consists of limestone and sandstone rock and crops out around Atfih water body. The undifferentiated Pliocene deposits consist of gravel, sand, and shale mapped in the northern part of the studied area. Moreover, the northern part of the Eastern Desert were investigated geologically, structurally, hydrogeologically, and land use map was created by using several data to illustrate the surface water of Atfih spring's position [43]. The clay outcrop of Kom El-Shelul formation contains deep marine Pliocene; placed in the north western part of surface water of Atfih spring was demonstrated using the seismic data along the Nile

valley by [41], [44]. Structurally, the studied area is affected by three main tectonic events including Syrian arc system, Gulf of Suez rift, and Mediterranean Sea system [45], [46]. These tectonic events caused formation of main trend of faults; dominant in the studied area are NW-SE, E-W, and NE-SW directions. The Eastern Desert of Egypt contains four main groundwater aquifers, such as the Quaternary Aquifer, Karst Aquifer, the Nubian Sandstone Aquifer System, and Basement Aquifer [36]. The studied area contains two aquifers, which are Quaternary and Karst Aquifers. The Quaternary (Pliocene) Aquifer in the studied area is composed of sandstone, limestone, gravel, and intercalation of shale. This aquifer crops out of surface water of Atfih spring. This aquifer overlies the Karst Aquifer, which consists of–limestone, marl, marly sand, and sandy lime, with many fractures widened due to the dissolution of carbonate rocks. Aquitard layer shale and claystone are intercalated within Karst Aquifer. Thus, the presence of fractures and faults enhances the movement of groundwater through aquifers. The precipitation from seasonal rainfall is considered the main source of recharge to Karst Aquifer. This Karst Aquifer is exposed in the studied area on the surface at some locations, and found in the sub-surface in some other locations [37], [47]. In the Atfih area, the Nubian Sandstone Aquifer System is not exposed, and is poorly defined. The whole succession of hydrogeologic units of the central Eastern Desert, including the studied area is shown in (Figure 3).

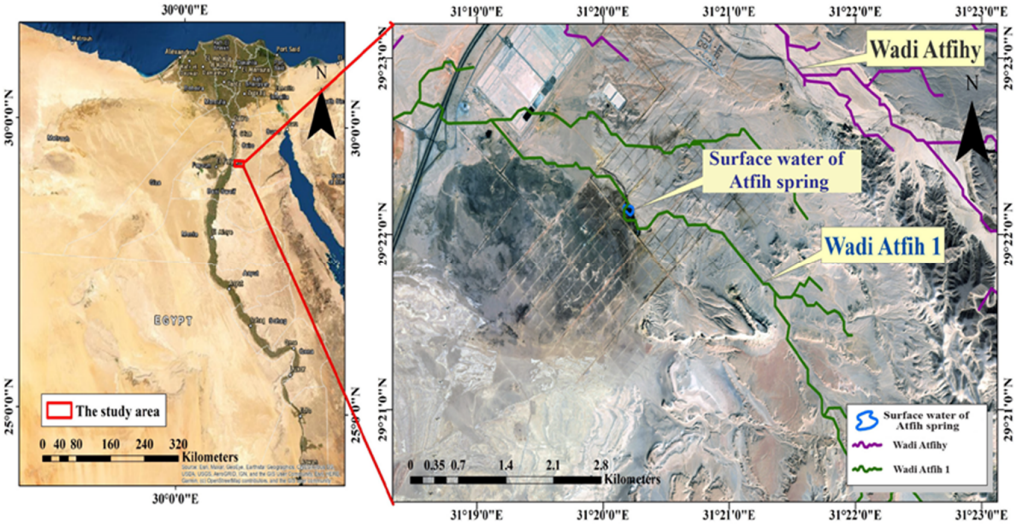

Figure 1. Location map of studied area.

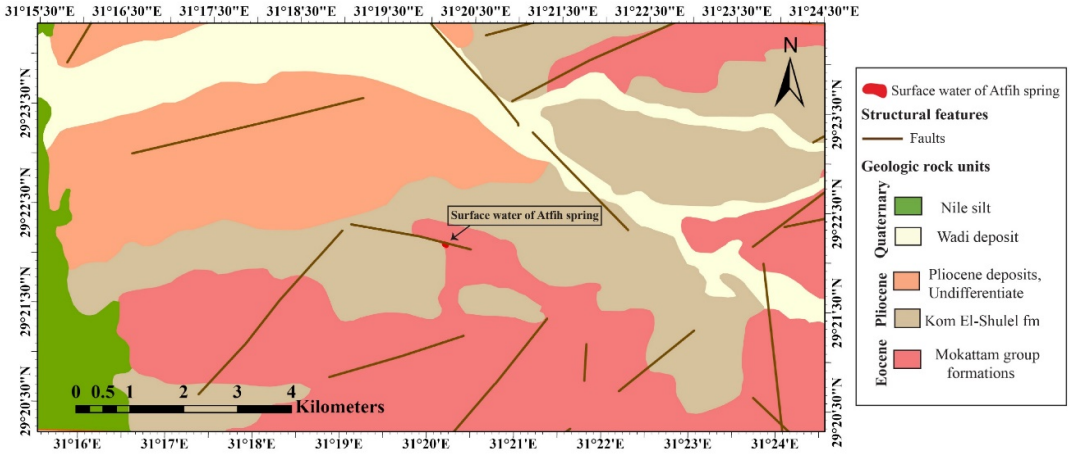

Figure 2. Geological map of studied area modified after [75].

The Quaternary Aquifer is recharged from the underlying deeper aquifers through sub-surface structure elements such as faults and fractures [48]; therefore, there is a hydrostatic connection between the different aquifers. Furthermore, rainfall flows westwards from the upstream of Wadi Atfih basin and other wadis to the Nile Valley and recharges the Quaternary Aquifer [49], [50]. The shallow aquifers to the south of the studied area are recharged from the Karst Aquifer, due to the presence of many fractures and faults that act as a conduit of water from one aquifer to another. Moreover, this Karst Aquifer is recharged by infiltrated rainfall water from seasonal rainy storms. Recently, a wastewater treatment station was constructed to the north west of Atfih spring; it has no effect on the surface water since; the slope is regional from east to west and spring at higher elevation to the east of the wastewater treatment station.

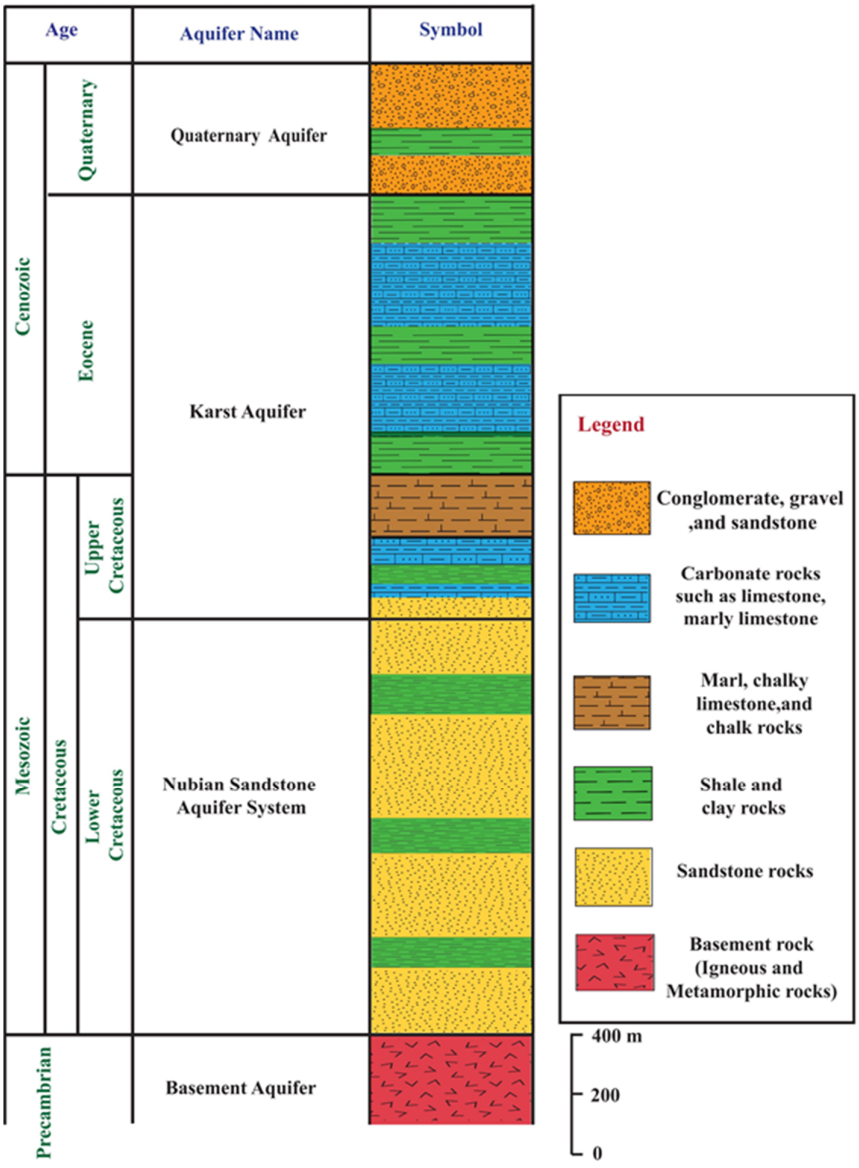

Figure 3. Hydrogeological stratigraphic sequence of the Eastern desert (modified after [76]).

4. Materials and Methods

Figure 4 shows the flow chart of the general methodology of the present study. Multi-temporal Landsat images, topographic maps, MERRA-2 precipitation data, and high-resolution images are prepared and analyzed to achieve the aims of the present study. Firstly, the MERRA-2 rainfall data was downloaded from NASA's website to

illustrate the relationship between the change in the surface water of Atfih spring area and the amount of precipitation. After that, Landsat satellite images were downloaded from the United States Geological Survey (USGS) Earth Explorer website with various sensors TM, ETM+, and OLI covered the studied region with path and raw (176, 40), respectively. This data was downloaded during specific years within the studied period from 1987 to 2019 to achieve the aim of extracting surface waterbody of Atfih spring. Landsat satellite images were utilized due to their advantages such as the ease of downloading and acquiring this data, and the availability of data during the stated study period. In addition, the simplicity of the processed raw data and its commercial cost. Preprocessing procedures for the Landsat data were applied to all downloaded multi-Landsat satellite scenes (Figure. 4). The main processing procedures include Normalized Difference Water Index (NDWI) and band ratios. The band ratio technique was applied in the studied region to construct the updated geological map. The lineaments were extracted manually to clarify the relationship between the geological structure feature and the emergence of surface water of Atfih spring. There are two methods for creating lineament extraction such as automatic and manual methods. The manual lineament extraction method was applied in the present study because the studied area contains several artificial line features; therefore, the lineament map was produced manually to be more reliable. In the present study, the high-resolution image with 0.5 m spatial resolution, field investigation, and Arc GIS 10.5v software tools were utilized to extract the lineaments in the studied region.

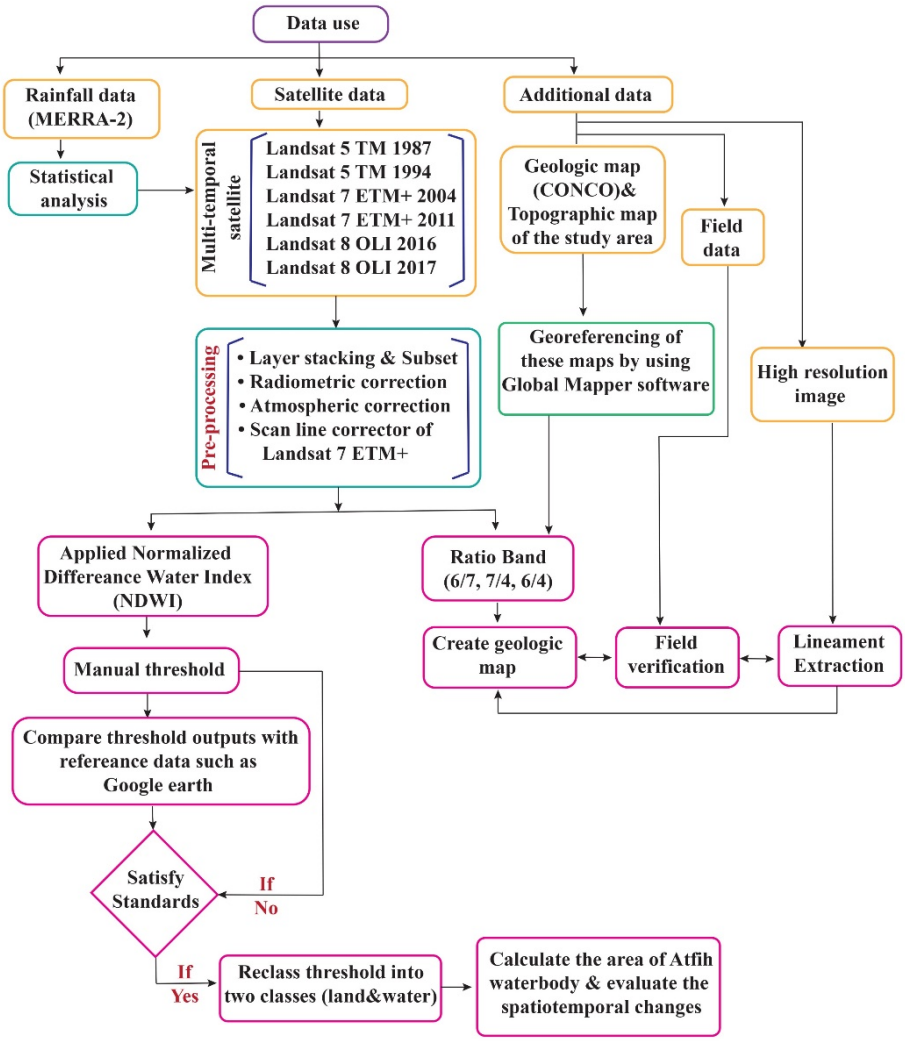

Figure 4. Flow chart of general methodology used in the present study.

5. Results and Discussion

5.1. Statistical analyses of MERRA-2 rainfall data

MERRA-2 is a new source of data that offers long-term air and surface measurements around the world[51]–[54]. It includes datasets in the period from 1980 to the present. The present study utilized monthly precipitation for the period from 1981 to 2019 of MERRA-2 project with a spatial resolution of 0.5° x 0.5° obtained from the NASA's website. After data analyses, many years were dropped, and the precipitation data of twenty years were selected for further analysis and visualization. Table 1 shows the main descriptive statistics of this data. The present study prepared and selected historical rainfall data (1981 to 2019) of MERRA-2 precipitation (mm day^{-1}) for analysis and visualization. Before starting the analyses, data reduction was performed. Only precipitation from 20 years was selected and years that received little or no precipitation were neglected. ANACONDA JUPITER NOTEBOOK for PYTHON code implementation was utilized. Two main visualization methods were selected to describe the precipitation data: heatmap and boxplot. Figure 5; shows the heatmap of the rainfall distribution. It clearly defines the months that received a high amount of precipitation. November is the rainy month over the studied area, in which four main storms were recorded. In November, the highest amounts of precipitation were recorded in 2016, 2017, 1994, and 1984, reaching about 116, 48, 19, and 18 (mm/day), respectively. Other high precipitation was recorded sporadically in October, December, January, and March occurred during 2016, 1987, and 1982, respectively. Figure 6 represents the boxplot of the precipitation data. It shows the main rainfall storms in this study, and the highest amount of precipitation amounts 116mm/day recorded in 2016.

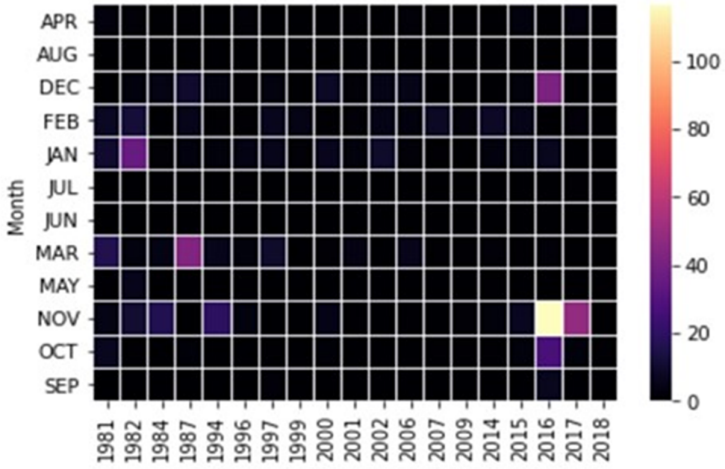

Figure 5. Heatmap for precipitation over studied area.

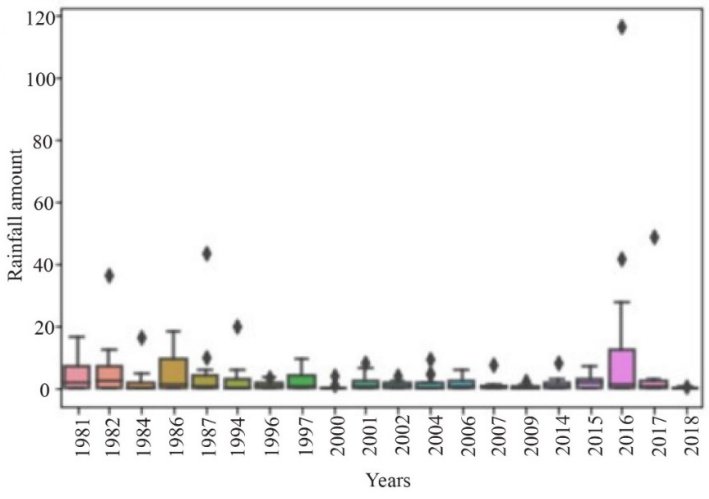

Figure 6. Box-plot of rainfall data shows the main storms.

Table 1. Descriptive statistics of the final selected precipitation data.

Min	Max	Mean	STDev	Skewness	Kurtosis
0	16.19	4.05	5.15	1.36	1.41
0	36.24	6.14	10.36	2.58	7.28
0	16.63	2.25	4.81	2.84	8.56
0	18.24	4.97	6.64	1.15	-0.17
0	43.53	5.42	12.38	3.11	10.12
0	19.84	2.71	5.69	2.89	8.9
0	3.76	1.14	1.34	1.21	0.12
0	9.12	2.28	3.09	1.26	0.51
0	4.14	0.5	1.18	3.13	10.13
0	8.39	1.95	2.92	1.43	0.77
0	4.02	0.92	1.28	1.54	1.82
0	9.49	1.68	3.05	1.91	3.09
0	5.69	1.56	2.05	1.17	0.2
0	7.86	0.97	2.19	3.31	11.23
0	2.49	0.43	0.72	2.39	6.3
0	8.19	1.4	2.38	2.44	6.53
0	6.94	2.03	2.33	0.98	0.17
0	116	16.77	33.96	2.67	7.55
0	48.59	4.81	13.83	3.42	11.78
0	0.81	0.19	0.26	1.55	1.89

5.2. Utilization of multi-temporal Landsat images to map changes of surface water of Atfih spring

Landsat multi-temporal images and geographic information system (GIS) were utilized to assess the change in the surface water of Atfih spring. The selected images were chosen and downloaded from USGS annually during the period (1987-2019) after one or two months of the maximum rainstorm occurred at each year (Table 2). The normalized difference water index (NDWI) was applied to the selected Landsat satellite data to extract the surface water of Atfih spring. The NDWI considered as type of ratio method that is described below:

$$NDWI = \frac{Green - NIR}{Green + NIR}$$

where NIR is a near-infrared band, and Green is a green band image of the Landsat satellite scenes. The NDWI thresholds separated the Landsat satellite image into the two classes water and land. The output vector of NDWI equation that represents the surface water of Atfih spring was extracted annually through the study period, and the area of the waterbody was calculated. The selection of the date of Landsat data used for evaluation depends on the number of rainfall storms. Years that received rainfall amounts less than 10 mm\day were neglected. Figures 7a, b, c, d, e, and f show the subset of the Atfih area with their polygons detecting the water body around Atfih Spring. The results show that when the quantity of extreme mean annual rainfall storms increased, the area of the surface water of Atfih spring enlarged. This direct relation between rainfall storm amount and the surface water of Atfih spring area change is clearly shown in (Figure 7) and (Table 2). There is an event of maximum mean annual precipitation storm that occurred in the studied area during the desired period in 2016, at which the area of Atfih waterbody increased to be 3649.86 m^2. This relation between the amount of rainfall and the formation of Atfih waterbody was clarified during the years of 1987 and 2016 (Figure 8a).

Table 2. Results of surface water areas of Atfih spring and amount of rainfall.

Year	Month of a maximum rainstorm	Month of acquired satellite data	Landsat satellite sensor	Spatial resolution of Green and near infrared bands	Amount of precipitation of this month (mm\day)	Area of surface water of Atfih spring by using NDWI index (m^2)
1987	March	April	Landsat 5 TM	30 m	43.53	1232.64
1994	Nov	Dec	Landsat 5 TM	30 m	19.84	1671.86
2004	Feb	Mar	Landsat7 ETM+	30 m	13.76	2331.69
2011	Jan	Mar	Landsat7 ETM+	30 m	11.62	2477.84
2016	Nov	Dec	Landsat 8 OLI	30 m	116.44	3649.86
2017	Nov	Dec	Landsat 8 OLI	30 m	48.59	2515.41

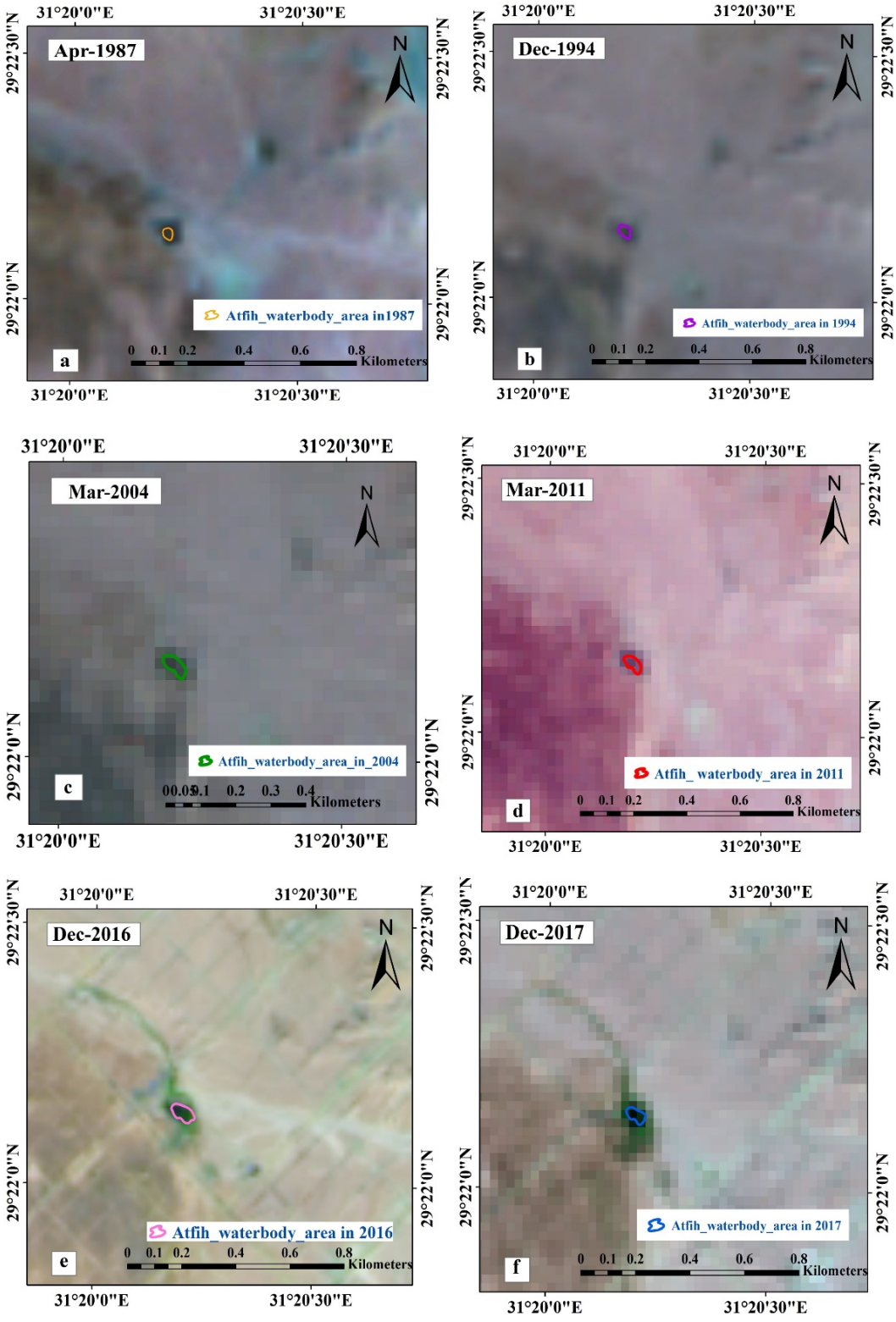

Figure 7. Atfih waterbody polygon that is extracted by using NDWI during years 1987, 1994, 2004, 2011, 2016, and 2017.

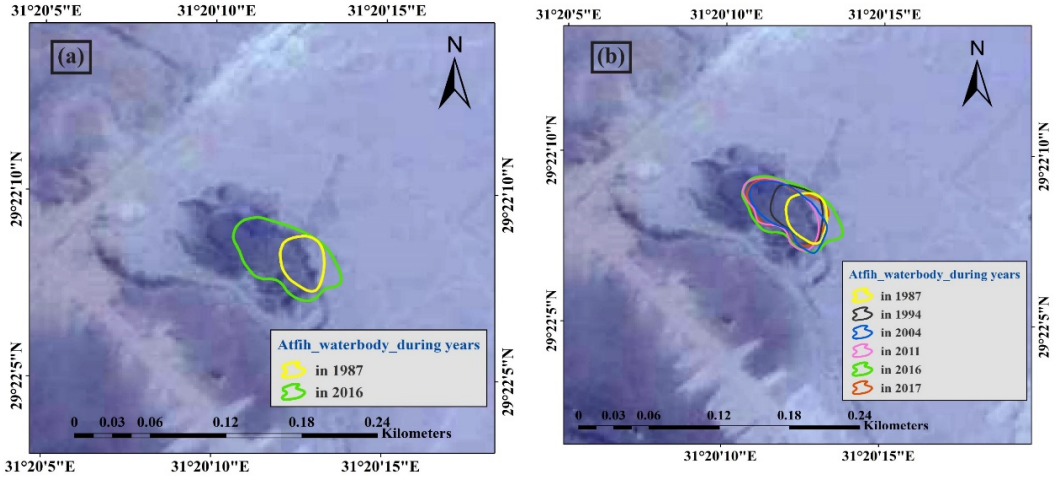

Figure 8. Change detection of Atfih waterbody surface area, (a) shows Atfih waterbody area during 1987 and 2016 years, and (b) illustrates the change of Atfih waterbody area during the selected years (1987, 1994, 2004, 2016, and 2017)

5.3. Factors controlling appearance of surface water of Atfih spring

Several researchers demonstrated the effect of lithology and structures for occurrence of springs that appear to the surface such as [55]–[57]. Field studies revealed that the lithology and geological structures are the main factors controlling the appearance of the surface water of Atfih spring. For lithologic discrimination, Landsat 8 OLI data was prepared and used.

5.3.1. Utilization of Landsat 8 OLI sensor for lithologic discrimination and updating geological map of Atfih area

In the current work, the Band Ratio technique was applied on Landsat 8 OLI to create a lithological map of the studied area. Although many researchers studied the lithological discrimination of the Eastern desert area by using Landsat satellite data such as[58]–[67], the lithologic discrimination using remote sensing data in Atfih area has not been studied before by any author. The band ratio technique was applied using Landsat 8OLI sensor because it could remove the effect of topography[68]. In the present study, the following band ratios (6/7, 7/4, 6/4, Figure 9) were effectively applied to discriminate the rock units covered the studied area. This band ratio image is distinct and competent for differentiating a range of geological rock units in the studied area such as the Quaternary deposit with dark green color, clay layer of Pliocene deposit (bright green), Pliocene deposit sandstone of Kom El-Shelul, and the Eocene carbonate of Mokattam Fm. However, the latter rock unit displays a multi-color in band ratio image since these deposits consist of three members: chalky limestone, marly limestone, and sandy limestone. Furthermore, band ratio of 6/7 on grayscale was used to discriminate the clay layer of Pliocene sediments from its surrounding (Figure 10). The clay deposit of Pliocene sediments is discriminated as darker color in (Figure 10) due to its high reflectance in band 7 and low reflectance and high absorption in band 6 [69]. The geologic map of the studied region was created by utilizing the integration between band ratio method and field survey data (Figure 11A).

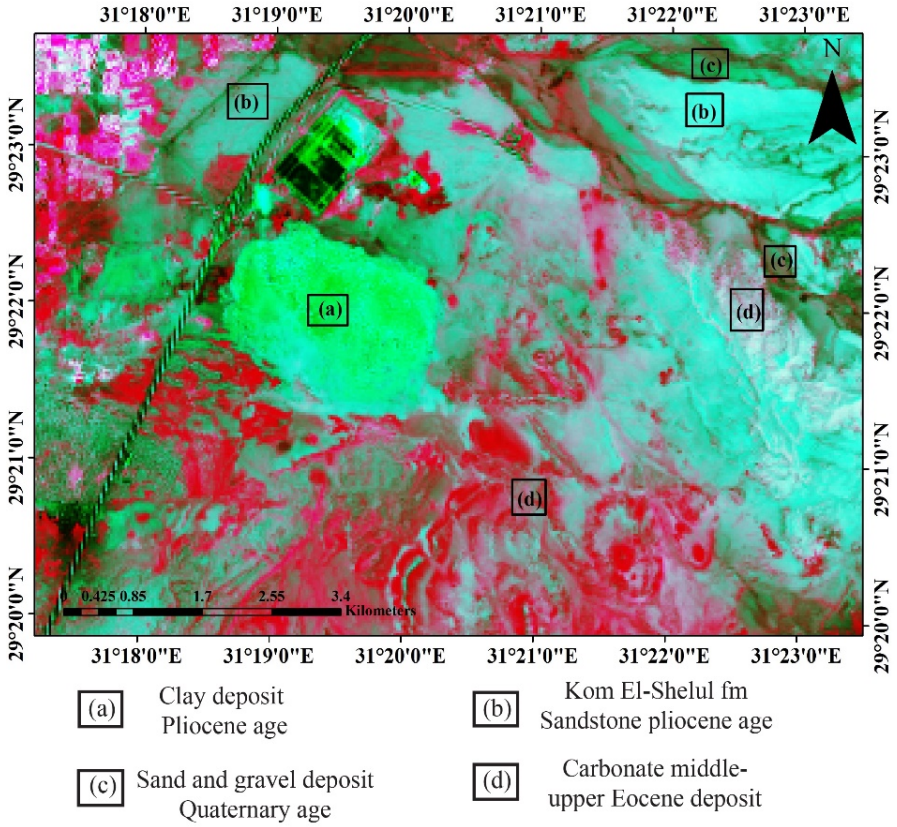

Figure 9. False color band ratios image 6/7, 7/4, 6/4 in RGB.

Figure 10. Band 6/band 7 ratio image in grayscale that discriminate clay layer of Pliocene deposit.

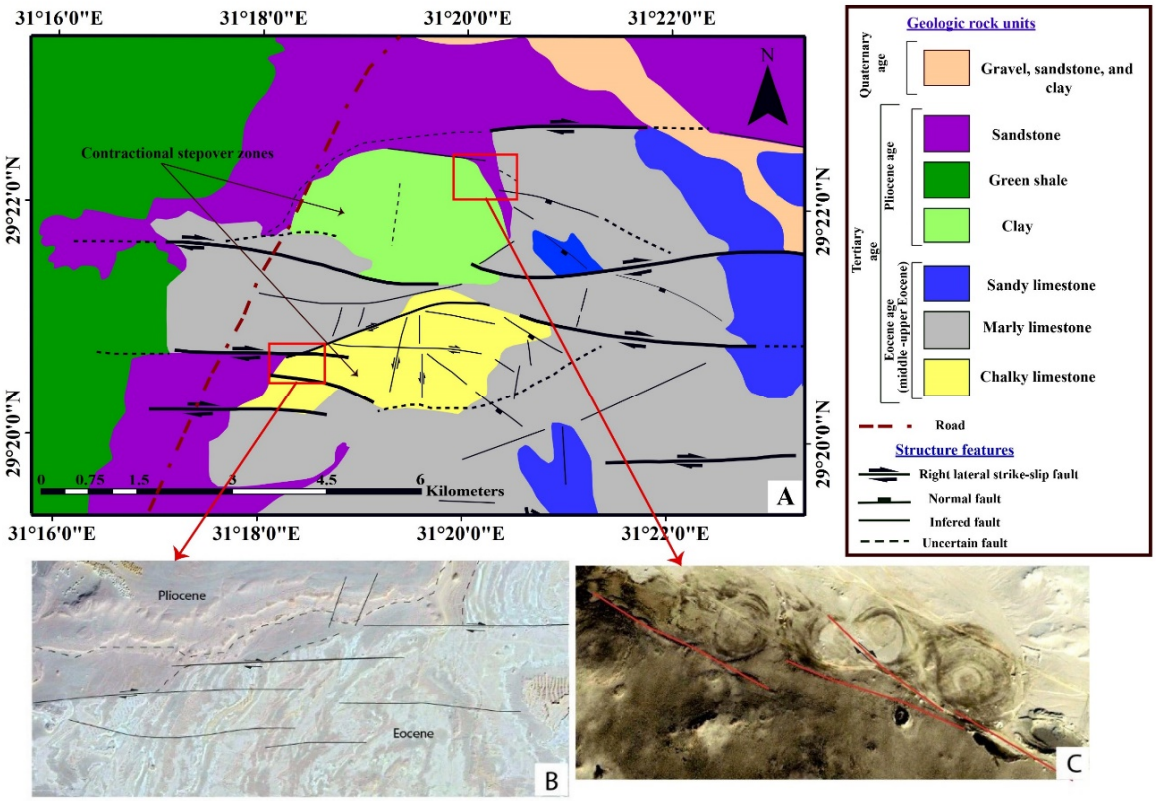

Figure 11. (A) Updated geological map of the studied area, (B) Satellite image illustrates the E-W right-lateral strike-slip fault, which caused the occurrence of transfer zone at Eocene deposit, and (C) Google Earth image shows the presence of faults at the Atfih spring location.

5.3.2. Structural setting and its role in formation of surface water of Atfih spring

The studied area lies in a tectonically complex setting; it has been affected by several tectonic phases starting with the Early Cretaceous rift of the Nile Valley basin [70]. Through the Late Cretaceous- Middle Eocene strike-slip tectonics (the age of fault in the current work) associated with the oblique convergent between Africa and Europe [71]–[74], and finally, the Oligo-Miocene extension associated with the opening of the Red Sea basin. The historical tectonic events mentioned above led to the formation of a network of faults and fractures with NW-SE, E-W to ENE-WSW, and NE-SW orientations on the eastern side of the surface water of Atfih spring (Figure11A). The NW and E-W oriented faults are extended for several kilometres on the Karst Aquifer to the east of the studied area, and greatly control the surface water flow and groundwater flow of the Karst Aquifer. E-W and ENE are the most dominant trends in the studied area, which are segmented right-lateral strike-slip fault system that encompasses several segments. Several small-scale folds of NE orientation were mapped along the deformation zone of the E-W fault segments (Figure 11C). Two major contractional stepover zone are developed as a linkage between the E-W fault segments. At mesoscale, these contractional step-over zones are marked by intensive fractured patterns including E-W, ENE, NW, and N-S orientations (Figure 12A). These highly fractured step-over zones act a crucial role in hydraulic connectivity along the studied area where they provide a seepage zone through the impermeable chalky limestone of the Middle Eocene. The fractures and connected fractures that exist in the field illustrated in (Figure 13).

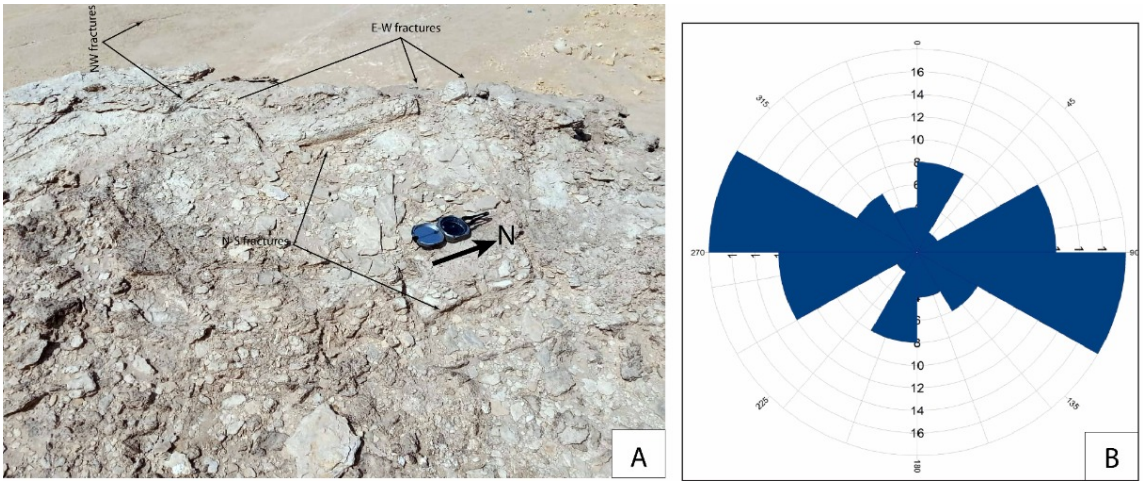

Figure 12. (A) Field photo showing the main trend of fractures that exist in the studied area. (B) Rose diagram shows the direction of dominant fractures.

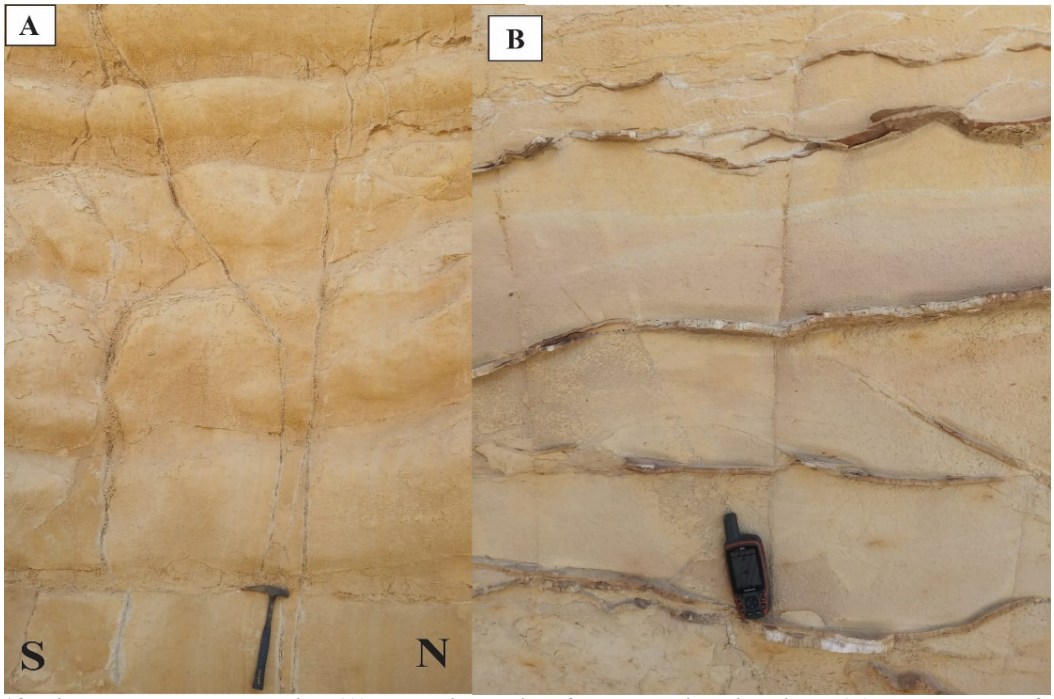

Figure 13. Field photographs showing (A) the main vertical fractures with directions. (B) the connected fractures that filled with gypsum due to flow of groundwater in the studied area.

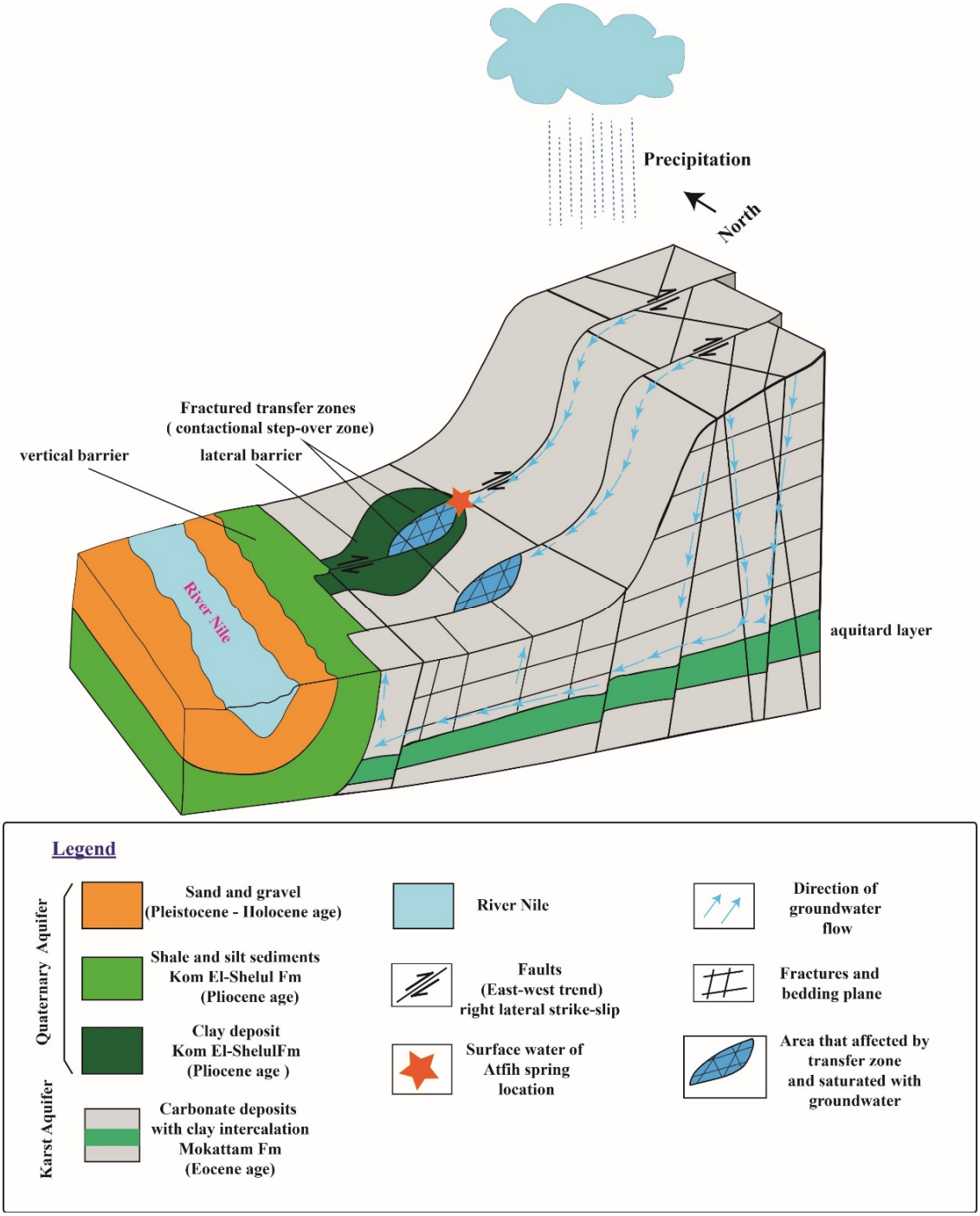

Figure 14. A 3D conceptual model illustrates occurrence of Atfih waterbody by presence of the transfer zone through faults that occurred in the Atfih studied area.

6. Conclusions

Population growth in Egypt has increased water demand. Many studies emphasized finding new unconventional water resources while conserving existing surface water. Remote sensing is utilized to extract surface water for human use. Surface water of Atfih spring lies close to the Atfih city in the Eastern Desert, Egypt. The present study demonstrated the change in this surface water and calculated the area that changed within the studied period (1987 – 2019) by using water indices such as NDWI. In addition, illustrated the reasons that caused the occurrence of this surface water. The result of MERRA-2 proved that the highest amount of precipitation was recorded in 2016, and the greatest area of the surface water of Atfih spring in

the same year. Therefore, the result of MERRA-2 rainfall data and the output of NDWI method indicate a relation between the precipitation amount and the change of surface water area of Atfih spring. When the rainfall quantity increases at Atfih upstream, the waterbody surface area increase. The lineaments extraction of structural features such as fractures and faults were applied to achieve the goal of this study; the result of extraction geologic structural features indicates that the right-lateral strike-slip faults with E-W and ENE trends that occurred in the studied area caused the formation of transfer zone. Moreover, the band ratio method was applied by using Landsat 8 OLI sensor to update the geological map of the study area. The result of the band ratio method clarifies that there are impervious layers such as shale and clay at the top surface and on the eastern side of the Nile Valley, which act as a barrier for the movement of water toward the Nile Valley. Thus, the groundwater in the Karst Aquifer recharged by precipitation has upward seepage to the surface, forming the surface water of Atfih spring.

A conceptual model for the occurrence of surface water of Atfih spring has been constructed (Figure 14). The model shows that rainfall precipitates in the upstream area of the Eocene carbonate plateau, followed by the infiltration of meteoric water downward through the fault network. This is to recharge the groundwater, which flows from East to West through the westward-tilted fractured Karst Aquifer. The thick shale succession of the Pliocene Kom El-Shelul formation, which juxtaposes the fractured Karst aquifer act as a lateral barrier and prevents debouching of the groundwater into Nile valley. The contractional step-over zones provide the vertical conduits for upward water flow at the vertical interface between the Pliocene shale and the Karst Aquifer. In conclusion, the results of this study indicate that the surface water of Atfih spring occurred according to the factors of lineaments and the amount of precipitation during the rainy season.

Acknowledgements

The authors would like to thank Mr. Ahmed Hammam and Mr. Ahmed Shawky for helping with the field work (Cairo University). Thanks to the United States Geological Survey (USGS) for the availability of Landsat satellite data for free. Thanks to the National Aeronautics and Space Administration (NASA) website for providing free MERRA-2 rainfall data. Special appreciation is extended to Ms. Maha Mark Muehlhauser (American University in Cairo) for editing the English language. Sincere appreciation to Cairo University for sponsoring our fieldwork for this project.

References

[1]. Sultan, S.A., Mansour, S.A., and Santos, F.A.M. (2008). A hydrogeophysical investigation of the Ain Mousa area, near Cairo, Egypt. Bulletin of Engineering Geology and the Environment, 67(1), 111-117.

[2]. Idris, H. (1996). Springs in Egypt. Environmental geology. 27 (2): 99-104.

[3]. Abdel Ghany, M. (1971). Hydrogeological Studies of Springs in the Area to the East of Cairo (Doctoral dissertation, M. Sc. Thesis, Fac. of Sc., Ain Shams Univ).

[4]. El Shamy, I. (2014). Helwan springs. In Thermal and Mineral Waters (pp. 91-96). Springer, Berlin, Heidelberg

[5]. Idris, M. (2000, May). Geothermal evaluation for thermal fluids of Helwan springs Egypt. In Proceedings World Geothermal Congress, Kyushu-Tohoku, Japan.

[6]. Abdalla, F.A., and Scheytt, T. (2012). Hydrochemistry of surface water and groundwater from a fractured carbonate aquifer in the Helwan area, Egypt. Journal of Earth System Science. 121 (1): 109-124, doi: 10.1007/s12040-012-0140-7.

[7]. El-Sayed, S.A., Morsy, S.M., and Zakaria, K.M. (2018). Recharge sources and geochemical evolution of groundwater in the Quaternary aquifer at Atfih area, the northeastern Nile Valley, Egypt. Journal of African Earth Sciences, 142, 82-92.

[8]. Enein, A.E., Khalil, M., Gedamy, Y., and Salem, H. (2017). Chemical and bacteriological impacts of wastewater on the water resources at Atfih Area, Giza Governorate, Egypt. Egyptian Journal of Chemistry. 60 (6): 1029-1043.

[9]. Morsy, S.M., and El-Sayed, S.A., (2018) Numerical groundwater flow and solute transport modeling for remediation of quaternary aquifer, north eastern desert, Egypt. pp. 131–149

[10]. Bense, V.F., Gleeson, T., Loveless, S.E., Bour, O., and Scibek, J. (2013). Fault zone hydrogeology. Earth-Science Reviews, 127, 171-192.

[11]. Caine, J.S., Evans, J.P., and Forster, C.B. (1996). Fault zone architecture and permeability structure. Geology. 24 (11): 1025-1028.

[12]. Joshi, B.K. (2006). Hydrology and nutrient dynamics of spring of Almora-Binsar area, Indian Central Himalaya: Landscapes, practices, and management. Water Resources. 33 (1): 87-96.

[13]. Bense, V.F., Person, M.A., Chaudhary, K., You, Y., Cremer, N., and Simon, S. (2008). Thermal

anomalies indicate preferential flow along faults in unconsolidated sedimentary aquifers. Geophysical Research Letters. 35 (24).

[14]. Burbey, T.J. (2008). The influence of geologic structures on deformation due to ground water withdrawal. Groundwater. 46 (2): 202-211.

[15]. Folch, A., and Mas-Pla, J. (2008). Hydrogeological interactions between fault zones and alluvial aquifers in regional flow systems. Hydrological Processes: An International Journal. 22 (17): 3476-3487.

[16]. Mayer, A., May, W., Lukkarila, C., and Diehl, J. (2007). Estimation of fault-zone conductance by calibration of a regional groundwater flow model: Desert Hot Springs, California. Hydrogeology Journal. 15 (6): 1093-1106.

[17]. Malaekeh, A., Ghassemi, M.R., Afzal, P., and Solgi, A. (2021). Fractal modeling and relationship between thrust faults and carbonate-hosted Pb-Zn mineralization in Alborz Mountains, Northern Iran. Geochemistry. 81 (4): 125803.

[18]. Madani, A., Gamal, M., and Ashour, A. (2005). Utilization of Landsat-7 ETM+ Imagery and seismic hazard assessment for the urban planning: a case study from El-Amal New City, East Cairo, Egypt. Egypt J Remote Sens Space Sci, 8, 3-20.

[19]. Abd El-Kawy, O.R., Rød, J. K., Ismail, H.A., and Suliman, A.S. (2011). Land use and land cover change detection in the western Nile delta of Egypt using remote sensing data. Applied geography. 31 (2): 483-494.

[20]. Butt, A., Shabbir, R., Ahmad, S.S., Aziz, N., Nawaz, M., and Shah, M.T.A. (2015). Land cover classification and change detection analysis of Rawal watershed using remote sensing data. J Biodivers Environ Sci. 6 (1): 236-248.

[21]. El-Sawy, E.S.K., Ibrahim, A.M., El-Bastawesy, M.A., and El-Saud, W.A. (2000). Detection of land use and land cover changes for New Cairo area, using remote sensing and GIS., doi: 10.21275/v5i2.nov161321.

[22]. Car, A. (2012). Change detection in land use land cover (LULC) in Međimurje county, Croatia, between 1978, 1992 and 2007 using Landsat satellite imagery (Doctoral dissertation, Salzburg University).

[23]. Im, N., Kawamura, K., Suwandana, E., and Sakuno, Y. (2015). Monitoring Land Use and Land Cover effects on water quality in Cheung Ek Lake using ASTER images. American Journal of Environmental Sciences. 11 (1): 1-12, doi: 10.3844/ajessp.2015.1.12.

[24]. Coppin, P.R., and Bauer, M.E. (1996). Digital change detection in forest ecosystems with remote sensing imagery. Remote sensing reviews. 13 (3-4): 207-234., doi: 10.1080/02757259609532305.

[25]. Kaliraj, S., Meenakshi, S.M., and Malar, V.K. (2012). Application of Remote Sensing in Detection of Forest Cover Changes Using Geo-Statistical Change Detection Matrices- A Case Study of Devanampatti Reserve Forest, Tamilnadu, India. Nature, Environment and Pollution Technology. 11 (2): 261-269.

[26]. Son, N.T., Chen, C.F., Chang, N.B., Chen, C.R., Chang, L.Y., and Thanh, B.X. (2014). Mangrove mapping and change detection in Ca Mau Peninsula, Vietnam, using Landsat data and object-based image analysis. IEEE Journal of Selected Topics in Applied Earth Observations and Remote Sensing. 8 (2): 503-510.

[27]. Du, Z., Bin, L., Ling, F., Li, W., Tian, W., Wang, H., and Zhang, X. (2012). Estimating surface water area changes using time-series Landsat data in the Qingjiang River Basin, China. Journal of Applied Remote Sensing. 6 (1): 063609, doi: 10.1117/1.jrs.6.063609.

[28]. Hossen, H., and Negm, A. (2016). Change detection of Manzala Lake using remote sensing and geographic information system. Egyptian Journal for Engineering Sciences and Technology, 19(EIJEST, Vol. 19, 2016): 353-358.

[29]. López-Caloca, A., Tapia-Silva, F.O., and Escalante-Ramírez, B. (2008). Lake Chapala change detection using time series. In Remote Sensing for Agriculture, Ecosystems, and Hydrology X (Vol. 7104, pp. 40-50). SPIE.

[30]. Ma, M., Wang, X., Veroustraete, F., and Dong, L. (2007). Change in area of Ebinur Lake during the 1998–2005 period. International Journal of Remote Sensing. 28 (24): 5523-5533.

[31]. Mohsen, A., Elshemy, M., and Zeidan, B.A. (2018). Change detection for Lake Burullus, Egypt using remote sensing and GIS approaches. Environmental Science and Pollution Research. 25 (31): 30763-30771.

[32]. Rokni, K., Ahmad, A., Selamat, A., and Hazini, S. (2014). Water feature extraction and change detection using multitemporal Landsat imagery. Remote sensing. 6 (5): 4173-4189., doi: 10.3390/rs6054173.

[33]. McFeeters, S.K. (1996). The use of the Normalized Difference Water Index (NDWI) in the delineation of open water features. International journal of remote sensing. 17 (7): 1425-1432.

[34]. Sarp, G., and Ozcelik, M. (2017). Water body extraction and change detection using time series: A case study of Lake Burdur, Turkey. Journal of Taibah University for Science. 11 (3): 381-391.

[35]. Korany, E.A., El-Ghazawi, M.M., and Faiad, B.J. (1997). Hydrographic analysis and hydrogeologic bearing of Wadi El-Atfihy, eastern Desert, Egypt-a case study of an ephemeral stream. Ain Shams Science Bulletin, 35, 73-88.

[36]. Abdel Moneim, A.A. (2005). Overview of the geomorphological and hydrogeological characteristics of the Eastern Desert of Egypt. Hydrogeology Journal. 13 (2): 416-425.

[37]. El Sayed, E.A. (1993). Hydrogeological studies of the Nile Valley in the northern portion of upper Egypt (Doctoral dissertation, Ph. D Thesis, Fac. Sci., El-Minia Univ., Egypt, 115p).

[38]. Korany, E.A., Soliman, M.M., and Faiad, B.J. (1997). Modeling of the hydrogeologic response of the Quaternary aquifer in the delta of El-Atfehy, eastern Desert, Egypt, and an assessment approach for development of groundwater resources. Ain Shams Sci. Bull, 35.

[39]. Said, R., (1962). The geology of Egypt (Amesterdam: Elsevier) 348p.

[40]. Saleh, A.S. (1990). Geomorphological effects of a torrential flood in wadi El-atfihy, the eastern desert of Egypt. The Bulletin of the Egyptian Geographical Society, 63, 99-128.

[41]. Said, R., (1990). The Geology of Egypt. A.A. Balkema, Rotterdam, Brook field, p. 450.

[42]. El-Saadawy, O., Gaber, A., Othman, A., Abotalib, A.Z., El Bastawesy, M., and Attwa, M. (2020). Modeling flash floods and induced recharge into alluvial aquifers using multi-temporal remote sensing and electrical resistivity imaging. Sustainability. 12 (23): 10204.

[43]. Nassar, T., (2018) Water Resources Management and Geoenvironmental Evaluation of Maaza Plateau Area , East of The Nile Valley , Egypt. unpublished PhD Thesis. Cairo university. P. 289.

[44]. Said, R. (1981). The Geological Evolution of the River Nile. viii + 151 pp., 73 Figures Berlin, Heidelberg, New York: Springer Verlag.

[45]. Farag, I.M., and Ismail, M.M. (1959). A contribution to the structure of the area east of Helwan. Egypt J Geol, 3, 71-86.

[46]. Soliman, S.M., and EA. K. (1980). Petrology of the Eocene near Cairo, Egypt.

[47]. Tantawy, M. (1992). Isotopic and hydrogeochemical applications to the surface and the groundwater assessments in El Minia district, Egypt (Doctoral dissertation, Ph. D. thesis, Faculty of Science, Minia University, Egypt).

[48]. Yousef, A.F. (2008). The Impact of North West Active Fault System on the Recharge of the Quaternary Aquifer System around the Nile Valley: Case Study Wadi El-Assiuty, Eastern Desert. Egypt. European Water. 21 (22): 41-55.

[49]. Awad, M.A., El Arabi, N.E., and Hamza, M.S. (1997). Use of solute chemistry and isotopes to identify sources of ground-water recharge in the Nile aquifer system, upper Egypt. Groundwater. 35 (2): 223-228.

[50]. Fiad, B.J. (1996). Hydrogeological Studies of the Groundwater Systems in the Qua- ternary Aquifer, Wadi El-Atfihy, Eastern Desert, Egypt. M. Sc. Thesis. Fac. Sci. Ain Shams Univ., Cairo, Egypt, p. 300.

[51]. Gelaro, R., McCarty, W., Suárez, M.J., Todling, R., Molod, A., Takacs, L. and Zhao, B. (2017). The modern-era retrospective analysis for research and applications, version 2 (MERRA-2). Journal of climate. 30 (14): 5419-5454.

[52]. Molod, A., Takacs, L., Suarez, M., and Bacmeister, J. (2015). Development of the GEOS-5 atmospheric general circulation model: Evolution from MERRA to MERRA2. Geoscientific Model Development. 8 (5): 1339-1356.

[53]. Suarez, M.J., Rienecker, M.M., Todling, R., Bacmeister, J., Takacs, L., Liu, H. C. and Nielsen, J.E. (2008). The GEOS-5 Data Assimilation System-Documentation of Versions 5.0. 1, 5.1. 0, and 5.2. 0 (No. NASA/TM-2008-104606-VOL-27).

[54]. Rienecker, M.M., Suarez, M.J., Gelaro, R., Todling, R., Bacmeister, J., Liu, E. and Woollen, J. (2011). MERRA: NASA's modern-era retrospective analysis for research and applications. Journal of climate. 24 (14): 3624-3648.

[55]. Taillefer, A., Soliva, R., Guillou-Frottier, L., Le Goff, E., Martin, G., and Seranne, M. (2017). Fault-related controls on upward hydrothermal flow: an integrated geological study of the Têt fault system, Eastern Pyrénées (France). Geofluids, 2017.

[56]. Issar, A., Rosenthal, E., Eckstein, Y., and Bogoch, R. (1971). Formation waters, hot springs and mineralization phenomena along the eastern shore of the Gulf of Suez. International Association of Scientific Hydrology. Bulletin, 16(3): 25-44.

[57]. Wannous, M., Theilen-Willige, B., Troeger, U., Falk, M., Siebert, C., and Bauer, F. (2021). Hydrochemistry and environmental isotopes of spring water and their relation to structure and lithology identified with remote sensing methods in Wadi Araba, Egypt. Hydrogeology Journal. 29 (6): 2245-2266.

[58]. Madani, A. (2000). Geological studies and remote sensing applications on Wadi Natash volcanics, Eastern Desert, Egypt. Unpublished Ph. D. Thesis, Faculty of Science, Cairo University.

[59]. Madani, A. (2012). Discrimination of Jurassic volcanicity in strike-slip basin, Jabal Al Maqtal area, South Eastern Desert, Egypt, using ASTER and field data. Earth Sci. 23 (2): 1-18.

[60]. Madani, A. (2015). Spectroscopy of olivine basalts using FieldSpec and ASTER data: A case study from Wadi Natash volcanic field, south Eastern Desert, Egypt. Journal of Earth System Science. 124 (7): 1475-1486.

[61]. Madani, A.A., and Emam, A.A. (2011). SWIR ASTER band ratios for lithological mapping and mineral exploration: a case study from El Hudi area, southeastern desert, Egypt. Arabian journal of Geosciences. 4 (1): 45-52.

[62]. Madani, A.A., Abdel Rahman, E.M., FA WZY, K.M., and Emam, A. (2003). Mapping of the hydrothermal alteration zones at Haimur gold mine area, South Eastern Desert, Egypt, using remote sensing techniques. Egyptian Journal of Remote Sensing and Space Sciences. 6 (2003): 47-60.

[63]. Emam, A., Hamimi, Z., El-Fakharani, A., Abdel-Rahman, E., Barreiro, J.G., and Abo-Soliman, M.Y. (2018). Utilization of ASTER and OLI data for lithological mapping of Nugrus-Hafafit area, South Eastern Desert of Egypt. Arabian Journal of Geosciences. 11(23): 1-22.

[64]. Gad, S., and Kusky, T. (2006). Lithological mapping in the Eastern Desert of Egypt, the Barramiya area, using Landsat thematic mapper (TM). Journal of African Earth Sciences. 44 (2): 196-202.

[65]. Hammam, A., Gaber, A., Abdelwahed, M., and Hammed, M. (2020). Geological mapping of the Central Cairo-Suez District of Egypt, using space-borne optical and radar dataset. The Egyptian Journal of Remote Sensing and Space Science. 23 (3): 275-285.

[66]. Hassan, S.M., and Sadek, M.F. (2017). Geological mapping and spectral based classification of basement rocks using remote sensing data analysis: The Korbiai-Gerf nappe complex, South Eastern Desert, Egypt. Journal of African Earth Sciences, 134, 404-418.

[67]. Mohy, H., Basta, F.F., Saber, S.G., and El Sobky, A.F.A. (2017). Using Landsat 8 and ASTER Data for lithological Discrimination and Mapping in Wadi Hamad area, North Eastern Desert, Egypt. J. Am. Sci, 13, 1-13.

[68]. Liu, J.G., and Mason, P.J. (2013). Essential image processing and GIS for remote sensing. John Wiley & Sons.

[69]. Harris, J.R., Rogge, D., Hitchcock, R., Ijewliw, O., and Wright, D. (2005). Mapping lithology in Canada's Arctic: application of hyperspectral data using the minimum noise fraction transformation and matched filtering. Canadian Journal of Earth Sciences. 42 (12): 2173-2193.

[70]. Selim, S.S. (2016). A new tectono-sedimentary model for Cretaceous mixed nonmarine–marine oil-prone Komombo Rift, South Egypt. International Journal of Earth Sciences. 105 (5): 1387-1415.

[71]. Moustafa, A.R., and Khalil, M.H. (1995). Superposed deformation in the northern Suez Rift, Egypt: relevance to hydrocarbons exploration. Journal of Petroleum Geology. 18 (3): 245-266.

[72]. Moustafa, A.R., and Khalil, S.M. (2020). Structural setting and tectonic evolution of the Gulf of Suez, NW red sea and Gulf of Aqaba Rift systems. In The geology of Egypt (pp. 295-342). Springer, Cham.

[73]. Sakran, S., Shehata, A.A., Osman, O., and El-Sherbiny, M. (2019). Superposed tectonic regimes in west Beni Suef basin, Nile Valley, Egypt: Implications to source rock maturation and hydrocarbon entrapment. Journal of African Earth Sciences, 154, 1-19.

[74]. Salem, E., and Sehim, A. (2017). Structural imaging of the East Beni Sueif Basin, north eastern Desert, Egypt. Journal of African Earth Sciences, 136, 109-118.

[75]. Conco, C. (1987). Geological map of Egypt, scale 1: 500,000. Geological Survey and Egyptian General Petroleum Corporation, Cairo.

[76]. Zahran, H., Elyazid, K.A., and Mohamad, M. (2011). Beni Suef Basin the key for exploration future success in Upper Egypt. Search and Discovery Article, 10351.

تشخیص تغییر آب سطحی چشمه عطفیه با اثر تلفیقی طوفان‌های بارندگی و سازه‌های زمین‌شناسی با استفاده از داده‌های لندست

دیمه سعد[1*]، احمد مدنی[1]، سعید سعید[1]، محمد مختار یحیا[2] و تامر نصار[1]

۱. دانشگاه قاهره، دانشکده علوم، گروه زمین شناسی، جیزه، مصر

۲. آزمایشگاه مرکزی پایش کیفیت محیطی، مرکز ملی تحقیقات آب، کناتر الخیریه، مصر

ارسال ۲۰۲۲/۱۲/۱۶، پذیرش ۲۰۲۳/۰۱/۲۰

* نویسنده مسئول مکاتبات: deemah@sci.cu.edu.eg

چکیده:

مرز شرقی دره نیل در جنوب قاهره با چشمه‌های متعدد و آب‌های سطحی مرتبط متمایز می‌شود، به عنوان مثال، عین السیره و حلوان و عطفیه. به جز مورد دوم، همه آنها در مناطق شهری منتشر شده بودند و به سختی توسط داده های سنجش از دور شناسایی شدند. بنابراین مطالعه آبهای سطحی چشمه عطفیه برای شناخت ماهیت سامانه چشمه نیل شرقی کلیدی است. تغییر در این آب‌های سطحی بر اساس ادغام بین تجزیه و تحلیل مکانی و زمانی تصاویر ماهواره‌ای چند طیفی و داده‌های بارندگی تحلیل گذشته نگر عصر مدرن برای تحقیقات و کاربردها (MERRA-2) از سال ۱۹۸۷ تا ۲۰۱۹ و تحقیقات میدانی شناسایی شده است. تجزیه و تحلیل شاخص دیفرانسیل آب نرمال شده نشان دهنده افزایش دو تا سه برابری مساحت بدنه آبی عطفیه طی سال‌های ۲۰۱۶-۲۰۱۷ است. نتایج به دست آمده ارتباطی را بین ظاهر آب سطحی چشمه عطفیه و میزان بارندگی روشن کرد. یکی دیگر از عوامل کنترل آب عطفیه که در این اثر بررسی شده است، ساختارهای زمین شناسی است. یک بررسی میدانی با کمک داده‌های ماهواره‌ای پردازش شده، حضور سه جمعیت گسل را نشان داد: WNW-ESE، E-W به ENE-WSW و NNE-SSW. گسل‌های E-W تا ENE گسل‌های اصلی هستند و تمایل به حرکت و لغزش به سمت راست دارند. این الگوی گسلی و شیل پلیوسن تأثیر بسزایی بر ظاهر توده آبی عطفیه دارد. این گسل‌ها به‌عنوان یک کانال افقی عمل می‌کنند که امکان حرکت جانبی آب را از طریق کربنات‌ها فراهم شده است و شارژ آب در این مناطق از طریق عبور از منطق بسیار شکسته‌شده رخ می‌دهد.

کلمات کلیدی: داده های چند زمانی لندست، بدنه آبی عطفیه، طوفان های بارندگی، سازه های زمین شناسی.